

# Dust mass-loss rates from AGB stars in the Fornax and Sagittarius dwarf Spheroidal galaxies

Eric Lagadec<sup>1\*</sup>†, Albert A. Zijlstra<sup>1,2</sup>, Mikako Matsuura<sup>3,4</sup>, J.W. Menzies<sup>2</sup>,  
Jacco Th. van Loon<sup>5</sup>, Patricia A. Whitelock<sup>2,6</sup>

<sup>1</sup> Department of Astronomy, University of Manchester, Sackville street, Manchester M601QD, UK

<sup>2</sup> South African Astronomical Observatory, PO Box 9, 7935 Observatory, South Africa

<sup>3</sup> Division of Optical and IR Astronomy, National Astronomical Observatory of Japan, Osawa 2-21-1, Mitaka, Tokyo 181-8588, Japan

<sup>4</sup> Department of Physics and Astronomy University College London Gower Street, London WC1E 6BT, UK

<sup>5</sup> Astrophysics Group, School of Physical & Geographical Sciences, Keele University, Staffordshire ST5 5BG, UK

<sup>6</sup> National Astrophysics and Space Science Programme, Department of Mathematics and Applied Mathematics, and Department of Astronomy, University of Cape Town, Rondebosch, 7701, South Africa

Accepted . Received 1988

## ABSTRACT

To study the effect of metallicity on the mass-loss rate of asymptotic giant branch (AGB) stars, we have conducted mid-infrared photometric measurements of such stars in the Sagittarius (Sgr dSph) and Fornax dwarf spheroidal galaxies with the 10- $\mu$ m camera VISIR at the VLT. We derive mass-loss rates for 29 AGB stars in Sgr dSph and 2 in Fornax. The dust mass-loss rates are estimated from the  $K - [9]$  and  $K - [11]$  colours. Radiative transfer models are used to check the consistency of the method. Published IRAS and Spitzer data confirm that the same tight correlation between  $K - [12]$  colour and dust mass-loss rates is observed for AGB stars from galaxies with different metallicities, i.e. the Galaxy, the LMC and the SMC.

The derived dust mass-loss rates are in the range  $5 \times 10^{-10}$  to  $3 \times 10^{-8} M_{\odot} \text{yr}^{-1}$  for the observed AGB stars in Sgr dSph and around  $5 \times 10^{-9} M_{\odot} \text{yr}^{-1}$  for those in Fornax; while values obtained with the two different methods are of the same order of magnitude. The mass-loss rates for these stars are higher than the nuclear burning rates, so they will terminate their AGB phase by the depletion of their stellar mantles before their core can grow significantly. Some observed stars have lower mass-loss rates than the minimum value predicted by theoretical models.

**Key words:** circumstellar matter – infrared: stars.

## 1 INTRODUCTION

Stars with initial mass in the range 0.8–8  $M_{\odot}$  go through an asymptotic giant branch (AGB) phase towards the end of their evolution. This evolutionary phase is dominated by strong mass loss. The star expels material at rates up to  $10^{-4} M_{\odot} \text{yr}^{-1}$ , eventually ejecting between 20 and 80 per cent of its initial main-sequence mass. This process is of great importance for the chemical evolution of our Galaxy. Mass loss from AGB stars contributes to around half of the gas recycled by stars (Maeder 1992), and is a dominant source of Galactic dust.

The mass-loss mechanism of AGB stars is a two-step process. First, shocks due to pulsations from the star produce gas over-densities in an extended atmosphere (e.g. Höfner et al. 1998). This triggers the formation of dust. Secondly, radiation pressure acceler-

ates the dust to the escape velocity. The gas is carried along through friction with the dust particles. Pulsations alone can explain mass-loss rates up to about  $10^{-7} M_{\odot} \text{yr}^{-1}$ , but the much higher rates observed require dust-driven winds (Bowen & Wilson 1991).

The importance of metallicity on the mass-loss rates of AGB stars is not well understood. In low metallicity environments less dust is expected to form, leading to lower predicted mass-loss rates. Theoretical work by Bowen & Willson (1991) predicts that for metallicities below  $[\text{Fe}/\text{H}] = -1$  dust-driven winds fail, and the wind becomes pulsation-driven. This would affect the evolution of a low metallicity host galaxy in two obvious ways. First the stellar dust production would be much reduced and therefore the composition of the material out of which new stars and planets were forming would be significantly different. Secondly the much weaker dust-driven winds allow the degenerate core of the AGB star to grow for longer, resulting in much higher masses for the remnant white dwarfs. In extreme cases, the core could reach the Chandrasekhar limit before mass loss terminates its evolution. The Bowen & Willson mass-loss rates predict the occurrence of AGB supernovae at

\* E-mail: eric.lagadec@manchester.ac.uk

† Based on observations collected at the European Southern Observatory, Chile (ESO Programme 075.D-0443(A))

very low metallicities (Zijlstra 2004). It is therefore important to test whether dust-driven winds exist at low metallicity.

Observations in the Magellanic Clouds and the Galaxy have shown that the dust mass-loss rates are smaller in the Magellanic Clouds. Assuming that the dust-to-gas ratio is a linear function of metallicity ( $[\text{Fe}/\text{H}] = -0.6$  (Venn 1999) and  $[\text{Fe}/\text{H}] = -0.3$  for the Small and Large Magellanic Clouds respectively) yields the conclusion that the total mass-loss rate (dust+gas) may be similar in the three galaxies (van Loon 2000, 2006), although this assumption may not be strictly correct, as the dust in the carbon stars comes from primary carbon. In order to obtain further constraints on the effect of metallicity on the mass-loss rates from AGB stars, and to know if dust-driven mass loss can occur at very low metallicities, we need to study the mass-loss rates from more metal-poor AGB stars.

The dusty circumstellar envelopes surrounding these AGB stars absorb the radiation from the central star and re-emit it in the thermal infrared. Observations at infrared wavelengths have enabled the study of mass-loss from Galactic and Magellanic Clouds AGB stars. Thanks to the sensitivity achievable with mid-infrared instruments on 8m class ground-based telescopes, it is now possible to perform such studies for AGB stars in more distant Local Group galaxies.

We thus observed AGB stars in the Fornax dSph (Fornax) and Sagittarius (Sgr dSph) dwarf spheroidal galaxies using the mid-infrared camera VISIR on the VLT (ESO, Chile). Fornax is a satellite galaxy of the Milky Way, at a distance of  $\sim 138$  kpc. Sgr dSph is located behind the Galactic disc and bulge at a distance of  $\sim 24$  kpc. It is currently being torn apart by tidal forces (Majewski et al. 2003). Those galaxies have low metallicities (see section 2). Furthermore the distances of both galaxies are quite well known, making an estimation of the mass-loss rates easier than it is for stars within the Galaxy.

## 2 OBSERVATIONS AND TARGET SELECTION

### 2.1 Target galaxies

We selected targets in two satellite galaxies of the Milky Way: the Sgr dSph and the Fornax Dwarf Spheroidal galaxy. Their distance moduli are taken as 17.02 mag for Sgr dSph (Mateo et al. 1995) and 20.66 mag for Fornax (Bersier 2000).

Sgr dSph is located behind the Galactic Bulge. It is a substantial galaxy, but it is being disrupted by the Milky Way: the tidal tails surround the Galaxy. The majority of its stellar population has a metallicity in the range  $[\text{Fe}/\text{H}] = -0.4$  to  $-0.7$  and an age of  $8.0 \pm 1.5$  Gyr (Bellazzini et al. 2006). Two of the four planetary nebulae in this galaxy have identical abundances of  $[\text{Fe}/\text{H}] = -0.55$  (Dudziak et al. 2000). The carbon stars discovered by Whitelock et al. (1996, 1999) are plausibly related to the same population as the planetary nebulae. A more metal-rich population with  $[\text{Fe}/\text{H}] = -0.25$  also exists (Zijlstra et al. 2006a; Bonifacio et al. 2004), although it may not be uniformly distributed over the galaxy. Finally, there is a minor, very metal-poor, population with  $[\text{Fe}/\text{H}] \sim -2$  which is seen in the globular clusters, but also in one tidal-tail planetary nebula.

Fornax shows similar mass and properties to Sgr dSph, but is too far from the Galaxy to suffer obvious tidal disruption. It also shows evidence for an extended period of star formation with the metallicity increasing over time. The younger population (at  $\sim 3 \cdot 10^8$  yr even younger than Sgr dSph) has a metallicity of

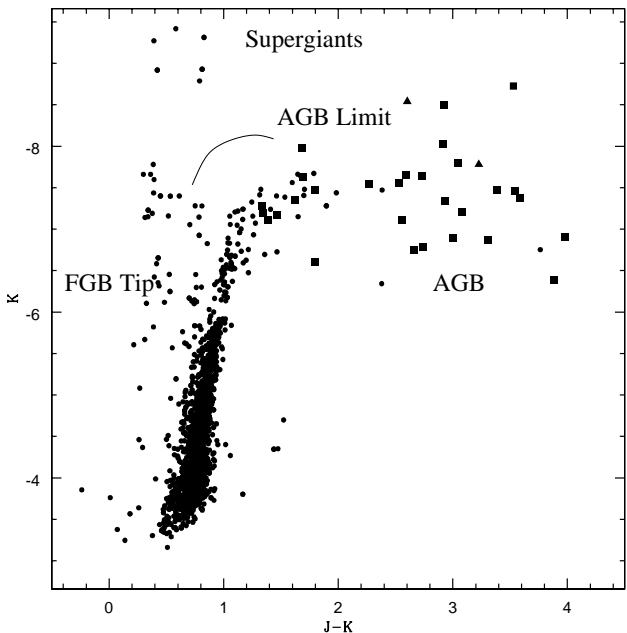


**Figure 1.** The  $M_{K_s}, J - K$  diagram of the observed sample. Squares represent the Sgr dSph stars and triangles the Fornax stars. Circles show the stellar population of Fornax (See Section 2.2 for more details).

$[\text{Fe}/\text{H}] = -0.7$  (Saviane et al. 2000) to  $\sim -0.6$  (Pont et al. 2004). The dominant population has an age of 2–10 Gyr and metallicity  $[\text{Fe}/\text{H}] = -1.0$  (Saviane et al.) or  $-0.9$  (Pont et al.). There is also a very metal-poor population as in Sgr dSph, with  $[\text{Fe}/\text{H}] \sim -2$ . The most metal-rich population is found mainly in the central regions.

### 2.2 Target selection

The targets within Sgr dSph (this galaxy subtends an angle of  $\sim 10^\circ$  in the sky and its center coordinates are  $\alpha(2000) = 18^h 55^m 04^s$  and  $\delta(2000) = -30^\circ 28' 42''$ ) were selected in two ways. First, we used the list of carbon stars given by Whitelock et al. (1999 — their table 1) with preference being given to the Miras with measured periods or to stars with near-infrared red colours; these are spectroscopically confirmed carbon stars. These are the stars with WMIF names in column 3 of Table 1. Secondly, stars were selected from the two micron all sky survey (2MASS) catalogue with the following properties:  $8 < K_s < 12$ ,  $2.6 < J - K_s < 4.5$ ,  $0.4(J - K_s) + 0.25 < J - H < 0.56(J - K_s) + 0.36$ . This selection should isolate carbon stars comparable to, or somewhat redder than, those discussed by Whitelock et al. and are a subset of those that have been monitored by Menzies et al. (in preparation) at  $JHK_s$  with the 1.4m Infrared Survey Facility (IRSF) at Sutherland. The carbon-rich nature of these stars has yet to be spectroscopically confirmed. Indeed it is not possible to disentangle oxygen-rich from carbon rich red AGB stars from JHK colours alone but in a low metallicity environment like Sgr, we expect more AGB stars to be carbon rich than in the Galaxy. All the stars with WMIF names in Table 1 have been confirmed as carbon stars from spectroscopy (Whitelock et al. 1999) and we will assume that all the other observed stars are carbon-rich, keeping in mind that some might be oxygen-rich. We will assume  $[\text{Fe}/\text{H}] \sim -0.55$ , based on the descendant PNe population (Zijlstra et al. 2006a) and the carbon-star population (Whitelock et al. 1996, 1999), but a range of metallicities

is probably represented. de Laverny et al. (2006) find for two Sgr dSph carbon stars (not observed by us)  $[M/H] = -0.5$  and  $-0.8$ .

Two carbon stars in Fornax were observed: these have similarly red colours to the Sgr dSph sample and are spectroscopically confirmed carbon stars (Matsuura et al. 2007). Both stars are located in the outer regions of Fornax ( $7'$  and  $15'$  from the centre). We assume that they have the  $[Fe/H] \sim -0.9$  of the dominant population, as the more metal-rich population is concentrated to the centre (Saviane et al. 2000).

We also observed the star IRAS 20176–1458, selected from Maun et al. (2004). This is a carbon star in the Galactic halo. All AGB carbon stars in the halo are expected to have escaped from one of the satellite galaxies, and the proximity of this star to the main body of Sgr dSph may indicate an association. Assuming an absolute magnitude of  $M_{bol} = -4$ , its distance is around 15 kpc which is not inconsistent with the tidal tail of Sgr (Law et al. 2005). The star lies several degrees off the location of the tidal stream (Majewski et al. 2003), but as noted by these authors, carbon stars may trace a different tidal event than the M stars. Maun et al. (2004) argue against an association with Sgr dSph.

The interstellar reddening towards Fornax is quite small,  $E(B - V) \sim 0.03$ , and thus negligible in  $K_s$  (Demers et al. 2002). For Sgr dSph, the reddening is estimated to be  $E(B - V) \sim 0.14$  (Layden & Sarajedini 2000). The reddening law from Rieke & Lebofsky (1985) yields  $(A_J, A_H, A_K) = (0.13, 0.09, 0.05)$ . The star Sgr01 is closer to the Bulge and may suffer a higher extinction: the NED model indicates  $E(B - V) = 0.24$  for this position.

The observed stars in both galaxies are shown in the (de-reddened)  $M_K$  vs  $J - K$  diagram in Fig. 1. Squares represent stars in Sgr dSph and triangles stars in Fornax. To show that the programme stars are on the AGB, we over-plotted the distribution of Fornax field stars: these data come from an unpublished survey using the 1.4m IRSF at Sutherland, and refer to a large area around the centre of Fornax. The tip of the red giant branch (RGB) is clearly visible, with a gap just above it showing the onset of hydrogen burning and thermal pulses.

Most of the selected stars have magnitudes consistent with thermal-pulsing AGB stars. They show a similar range to the mass-losing AGB stars in the SMC (Lagadec et al. 2007), but tend to be located towards the fainter end of those stars, with only three stars above  $M_K = -8$ .

### 2.3 VISIR observations

The observations were made with the VLT spectrometer and imager for the mid-infrared (VISIR, Lagage et al. 2004), located at the Cassegrain focus of the Very Large Telescope (VLT) UT3 at Paranal, Chile. The settings of our observations gave a  $0.075''$  per pixel scale and a field of view of  $32.5'' \times 32.5''$ . These observations were carried out in visitor mode during 4 nights from the 24th to the 28th of July 2005. We observed 29 AGB stars in Sgr dSph, 2 in Fornax and 1 in the Galactic halo. Some observations were repeated if the first measurement was made in poor seeing conditions. The log of the observations is presented Table 1.

The observations were affected by unstable weather: approximately half the time was non-photometric and could not be used. Seeing as reported by the optical seeing monitor varied between 0.4 and 3 arcsec.

To reduce the background emission from the sky and the telescope, we used the standard mid-infrared technique of chopping and nodding. To avoid saturation of the detector by the ambient photon background, each individual nod cycle was split into many

short exposures of  $\sim 10$ ms each. This procedure was repeated for as many cycles as needed to obtain sufficient signal-to-noise.

The data reduction was performed using our own IDL routines. Images were corrected for bad pixels, and then co-added to produce a single flat-field corrected image, comprising the average of the chop and nod differences. Standard stars were observed and analysed in the same way to flux-calibrate our observations. The flux calibration was performed using standard aperture photometry methods, applied to the programme and reference stars.

We observed all the stars with the VISIR PAH1 filter ( $\lambda_c = 8.59 \mu\text{m}$ ,  $\Delta\lambda = 0.42 \mu\text{m}$ ). The brighter stars were also observed with the VISIR PAH2 filter ( $\lambda_c = 11.25 \mu\text{m}$ ,  $\Delta\lambda = 0.59 \mu\text{m}$ ). The filters were selected for their very good sensitivity: they avoid the telluric ozone band. The zero-points for the two filters are taken as 53.7 ( $8.59 \mu\text{m}$ ) and 31.5 Jy ( $11.25 \mu\text{m}$ ) respectively (values taken for a blackbody with  $T_{eff} = 10000\text{K}$  and using Vega as a reference). The magnitudes derived using these zero-points are designated below as [9] and [11] respectively.

The measured magnitudes, together with the 2MASS or SAAO *JHK* photometry, are listed in Table 2. For comparison, we also list the IRAS [12] magnitude, taken from the Faint Source Catalogue (FSC), available for six sources. The IRAS magnitude is not colour-corrected. The IRAS magnitudes are in most cases a little brighter, by a few tenths of a magnitude. The IRAS filter extends to longer wavelengths than the VISIR filter, and the IRAS detected stars are red. The photometry is accurate to better than  $\pm 0.05$  mag at *JHK* for the stars observed at SAAO and around  $\pm 0.02$ - $0.03$  mag for the stars observed with 2MASS.

Fig. 2 shows the relation between the  $J - K$  colour and the  $K - [9]$  and  $K - [11]$  colours. Stars in Sgr dSph are shown corrected for interstellar reddening (using the values listed in section 2.2, with a higher value for Sgr01). Stars with  $J - K < 2$  exhibit little reddening and on average only a small mid-infrared excess. Among the blue stars, only Sgr13 shows significant excess flux at  $9 \mu\text{m}$ .

For redder stars, the  $J - K$  colour and the mid-infrared excess show correlated evidence for circumstellar dust.

The lower panel shows the  $[9] - [11]$  colour as function of  $J - K$ . The observations show no clear trend, although a trend does appear when the stars are separated on the basis of their  $9 \mu\text{m}$  magnitude. The open squares show the Sgr dSph stars with  $[9] > 6$  and the closed squares those with  $[9] < 6$ . The brighter stars generally have redder  $J - K$  colours. This can be understood as more dust (brighter [9]) resulting in higher optical depths and thus more reddening at  $J - K$ .

### 2.4 Bolometric magnitudes

The *JHK* magnitudes and the bolometric corrections derived by Whitelock et al. (2006) were used to estimate the apparent bolometric magnitudes of the programme stars:

$$BC_K = +0.972 + 2.9292 \times (J - K) - 1.1144 \times (J - K)^2 + 0.1595 \times (J - K)^3 - 9.5689 \times 10^{-3} (J - K)^4. \quad (1)$$

Because this equation is based on magnitudes from the SAAO system, we converted all the photometry to the SAAO system and then reddening corrected it. The absolute bolometric magnitudes were then calculated assuming distance moduli of 17.02 for Sgr dSph (Mateo et al., 1995) and 20.66 for Fornax (Bersier 2000). The results for the Sgr dSph stars are listed in Table 2.

The histogram of the luminosity distribution is shown in Fig. 3. The tip of the RGB (TRGB) is also indicated, using the cal-

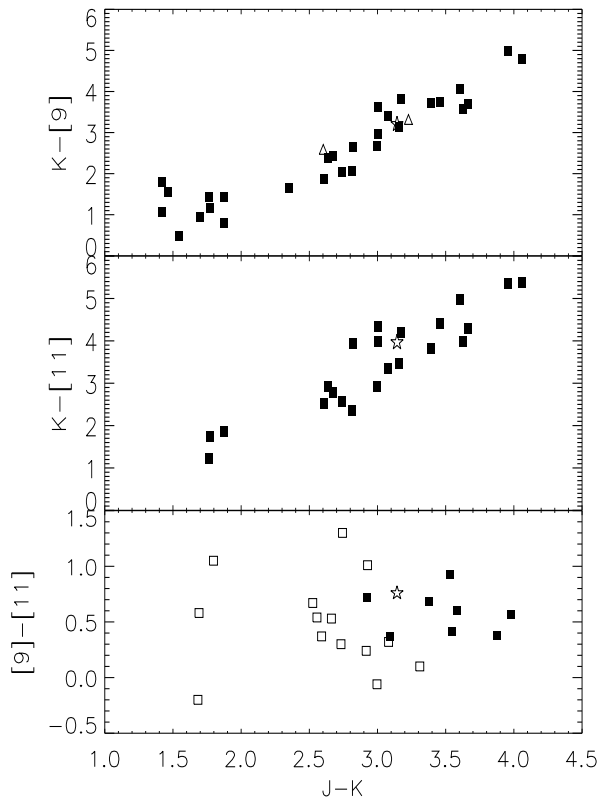


**Figure 2.** The interstellar reddening-corrected  $J - K$  colours versus the mid-infrared excess. Squares are the Sgr dSph stars; triangles are the two stars in Fornax and the star symbol represents the Galactic halo carbon star. The lower panel shows the  $[9] - [11]$  colour, where the filled squares show Sgr dSph stars with  $[9] < 6$  mag and the open squares the fainter stars.

ibration of Bellazzini et al. (2001). The large majority of stars are within one magnitude of this tip. One star (Sgr27) is significantly below the TRGB (by  $\sim 0.7$  mag).

### 3 METHODS TO DETERMINE MASS-LOSS RATES FROM INFRARED COLOURS

The mid-infrared colours can be used to obtain mass-loss rates from these AGB stars. From a survey of Miras in the South Galactic Cap, Whitelock et al. (1994) showed that the mass-loss rates and the  $K - [12]$  colour are tightly correlated, where  $[12]$  is the IRAS  $12\mu\text{m}$  magnitude (see fig. 21 in their paper). This can be understood from the fact that the  $K$  magnitude is a measure of the emission from the star, while the  $[12]$  magnitude a measure of emission from dust in the circumstellar envelope. The  $K - [12]$  colour will thus increase with mass-loss rate.

Mass-loss rates from Galactic AGB stars have also been estimated using dust radiative transfer models (e.g., Le Bertre 1997). For these models, a dust composition is assumed, as well as a dust grain size, a density distribution, an expansion velocity for the envelope, and a temperature and luminosity for the central star. The optical depth is a free parameter. The best fit model of the observed SED gives an estimate of the optical depth of the dusty envelope. If we assume that dust is composed of spherical grains of a given composition and size, we can determine their optical properties using Mie theory. The expansion velocity of circumstellar envelopes

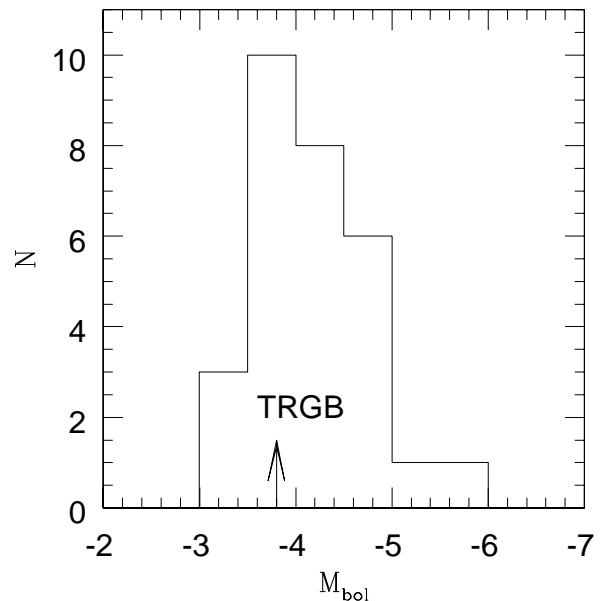


**Figure 3.** Distribution of bolometric magnitudes of the observed stars in Sgr dSph, assuming a distance modulus of 17.02.

of Galactic AGB stars have been estimated using CO observations (e.g., Loup et al. 1993). Thus by determining the optical depths of the envelopes, we can estimate mass-loss rates. The values estimated with these dusty radiative transfer models are consistent with those derived from the CO emission line measurements (e.g., Le Bertre 1997). For more information about infrared methods to determine mass-loss rates from AGB stars, we refer to the review by van Loon (2006).

## 4 METHODS FOR DETERMINING THE MASS-LOSS RATE

### 4.1 Method 1: calibrated colour relations

#### 4.1.1 Calibration

As mentioned in Section 3, a tight correlation exists between the  $K - [12]$  colour and the mass-loss rates for Galactic AGB stars (Whitelock et al. 1994). Here, the  $12\mu\text{m}$  magnitude represents the broad-band IRAS measurement. The Whitelock et al. sample contains 58 O-rich stars and only 3 C-rich stars. Using a further sample of 239 Galactic C-rich stars, Whitelock et al. (2006) determined the correlation between  $K - [12]$  and mass-loss rates for C-rich AGB stars. This relation was quantified as:

$$\begin{aligned} \log(\dot{M}_{\text{total}}) &= -7.668 + 0.7305(K - [12]) \\ &\quad - 5.398 \times 10^{-2}(K - [12])^2 \\ &\quad + 1.343 \times 10^{-3}(K - [12])^3 \end{aligned} \quad (2)$$

Our observations used VISIR filters with wavelengths close to  $12\mu\text{m}$ . The two filters, selected because of their high sensitivity, have wavelengths centred at  $8.59$  and  $11.25\mu\text{m}$ . To derive an equivalent relation to Eq. 2 for these filters, we retrieved all the available IRAS LRS spectra used by Whitelock et al. (2006). We then convolved these spectra with the VISIR transmission curves for the filters used. We also convolved them with the IRAS  $12\mu\text{m}$

**Table 1.** Log of the observations. Names and adopted coordinates.  $t_{\text{PAH1}}$  and  $t_{\text{PAH2}}$  are the exposure time using the filters centred at 8.59 and 11.25 $\mu\text{m}$  respectively. Stars with names beginning with WMIF in column 3 are taken from the sample of Whitelock et al. (1999).

Star number	2MASS name	Previous name	RA	Dec (J2000)	t PAH1 s	t PAH2 s	Ref star
<b>Sgr dSph</b>							
Sgr01	18405750–2734227		18 40 57.5	–27 34 22.7	90.16	90.62	HD119193
Sgr02	18414350–3307166	IRAS 18384–3310	18 41 43.50	–33 07 16.6	180.32	181.24	HD169916
Sgr03	18443095–3037098	IRAS 18413–3040	18 44 30.96	–30 37 09.8	180.32	181.24	HD169916
Sgr04	18450563–2915574		18 45 05.64	–29 15 57.4	90.16	90.62	HD169916
Sgr05	18463228–2953484		18 46 32.3	–29 53 48.4	180.32	59.1	HD169916
Sgr06	18463912–3045527	WMIF-C02	18 46 39.12	–30 45 52.7	1081.92	1449.92	HD169916
Sgr07	18465160–2845489	IRAS 18436–2849	18 46 51.6	–28 45 48.9	90.16	90.62	HD181109
Sgr08	18511108–3121563		18 51 11.08	–31 21 56.3	360.64	362.48	HD169916
Sgr09	18514105–3003377		18 51 41.05	–30 03 37.7	90.16	90.62	HD177716
Sgr10	18524416–3121150		18 52 44.16	–31 21 15.0	90.16	90.62	HD169916
Sgr11	18525030–2956317	WMIF-C04	18 52 50.7	–29 56 30.6	540.96	634.34	HD181109
Sgr12	18534097–2934228		18 53 40.98	–29 34 22.9	90.16	90.62	HD169916
Sgr13	18542429–3025105	WMIF-C06	18 54 24.29	–30 25 10.6	721.28	226.55	HD177716
Sgr14	18532937–2938241	WMIF-C05	18 53 29.38	–29 38 24.2	1803.2		HD169916
Sgr15	18584385–2956551	IRAS 18555–3001	18 58 43.85	–29 56 55.1	90.16	90.62	HD181109
Sgr16	19000215–3035347	IRAS 18568–3039	19 00 02.15	–30 35 34.7	90.16	90.62	HD181109
Sgr17	19015287–3032391	WMIF-C15	19 01 52.88	–30 32 39.2	270.48	362.48	HD169926
Sgr18	19043562–3112564	IRAS 19013–3117	19 04 35.62	–31 12 56.4	90.16	90.62	HD181109
Sgr19	19044898–3110540	WMIF-C17	19 04 48.98	–31 10 54.0	360.64	362.48	HD169916
Sgr20	19065718–3412371		19 06 57.18	–34 12 37.1	450.80	724.96	HD181109
Sgr21	19093902–2956561	WMIF-C18	19 09 39.03	–29 56 56.1	721.28	634.340	HD169916
Sgr22	19103987–3228373	IRAS 19074–3233	19 10 39.87	–32 28 37.3	90.16	90.62	HD177716
Sgr23	19125006–3051228		19 12 50.06	–30 51 22.8	90.16	90.62	HD177716
Sgr24	19165541–3248289		19 16 55.41	–32 48 28.9	180.32	453.1	HD181109
Sgr25	19232461–3400149	WMIF-C22	19 23 24.61	–34 00 15.0	1803.2		HD169916
Sgr26	19234548–3431150	WMIF-C23	19 23 24.48	–34 31 15.0	1803.2		HD169916
Sgr27	19313851–3002305	WMIF-C25	19 31 38.5	–30 02 30.5	1803.2		HD177716
Sgr28	19425082–3334333	WMIF-C26	19 42 50.83	–33 34 33.3	721.28		HD177716
Sgr29	19485065–3058317		19 48 50.65	–30 58 31.9	90.16	90.62	HD181109
<b>Fornax</b>							
For1	02385056–3440319		02 38 50.56	–34 40 31.9	2163.84		HD16815
For2	02391232–3432450		02 39 12.33	–34 32 45.0	1803.20		HD16815
<b>Halo</b>							
Halo1	20202766–1449272	IRAS 20176-1458	20 20 27.66	–14 49 27.1	90.16	90.62	HD177716

filter, and scaled the spectra such that the catalogued IRAS 12 $\mu\text{m}$  flux was recovered. The [9] and [11] magnitudes of the Galactic C-stars were obtained using the zero-points listed in Table 2.

The  $K$  band flux of the stars we observed in Sgr dSph and Fornax have been measured either with 2MASS ( $K_{\text{S2MASS}}$ ) or at the SAAO ( $K_{\text{SAAO}}$ ). To obtain a uniform flux measurement for the  $K$ -band we transformed the SAAO measurements to the 2MASS photometric system, following (Carpenter 2001):

$$K_{\text{S2MASS}} = K_{\text{SAAO}} + 0.020(J - K)_{\text{SAAO}} - 0.025 \quad (3)$$

This was done for all stars in the Whitelock et al. (1994, 2006) samples. The resulting colours were plotted against the dust mass-loss rate taken from the Whitelock et al. papers.

The result for the carbon-rich sample of Whitelock et al. (2006) is shown in Fig. 5: there is a good correlation between the  $K_s - [9]$  and  $K_s - [11]$  colours and the dust mass-loss rates. The oxygen-rich stars of Whitelock et al. (1994) show a similar relation (Fig. 5) but extending to less red colours. The relation holds for  $K_s - [9] < 7$  and is a consequence of dust emission at 10 $\mu\text{m}$  and dust opacity in the  $K_s$ -band.

Note that Whitelock et al. derived total mass-loss rates (dust+gas), adopting a gas-to-dust mass ratio of 200. As what we observed at 9 and 11 $\mu\text{m}$  is mostly due to emission from dust, we determine dust mass-loss rates. The gas-to-dust mass ratios in the envelope of AGB stars in the observed galaxies being poorly known, we prefer to discuss dust mass-loss rates.

The relations between colours and mass-loss rates for these Galactic AGB carbon stars can be quantified as:

$$\log(\dot{M}_{\text{dust}}) = -9.41 + 0.27(K_s - [9]) + 0.05(K_s - [9])^2 - 0.0055(K_s - [9])^3 \quad (4)$$

and:

$$\log(\dot{M}_{\text{dust}}) = -9.58 + 0.26(K_s - [11]) + 0.05(K_s - [11])^2 - 0.0053(K_s - [11])^3 \quad (5)$$

To check the dependence of this relation on metallicity, we determined the equivalent relations for stars in the Small and Large Magellanic Clouds (hereinafter SMC and LMC), which we assume to have lower metallicity than similar stars in the Milky Way. Re-

**Table 2.** Sgr dSph and Fornax photometry. For stars with names beginning with WMF (Whitlock et al. 1999) in column 3 of Table 1, the  $JHK$  photometry comes from unpublished data taken at SAAO on the 1.9m telescope (SAAO in last column), and, where multiple observations are available, refers to the mean magnitude. For all other stars (2MASS in last column), the  $JHK_s$  is taken from 2MASS. All  $JHK_s$  magnitudes are given on the 2MASS photometric system. PAH1 and PAH2 represent our VISIR observations at 8.59 and 11.25 $\mu\text{m}$  respectively. Zero-points are taken to be 53.7 (8.59 $\mu\text{m}$ ), 31.5 (11.59 $\mu\text{m}$ ) and 28.3 Jy (IRAS).

Star number	$J$ mag	$H$ mag	$K_s$ mag	PAH1 mag	PAH2 mag	$M_{bol}$ mag	IRAS [12] mag	$JHK_s$ observations
<b>Sgr D</b>								
Sgr01	12.479	10.774	9.308	5.48 $\pm$ 0.03	5.11 $\pm$ 0.03	-4.66		2MASS
Sgr02	11.577	9.971	8.575	4.96 $\pm$ 0.02	4.24 $\pm$ 0.03	-5.29	3.90	2MASS
Sgr03	13.236	11.183	9.612	6.03 $\pm$ 0.04	5.62 $\pm$ 0.06	-4.67	5.50	2MASS
Sgr04	12.250	10.708	9.438	7.38 $\pm$ 0.12	7.08 $\pm$ 0.24	-4.33		2MASS
Sgr05	13.027	11.319	9.866	6.73 $\pm$ 0.05	6.41 $\pm$ 0.16	-4.09		2MASS
Sgr06	11.481	10.315	9.604	8.80 $\pm$ 0.08	7.75 $\pm$ 0.09	-3.99		SAAO
Sgr07	13.060	11.123	9.599	5.86 $\pm$ 0.04	5.18 $\pm$ 0.05	-4.56	4.84	2MASS
Sgr08	13.062	11.528	10.320	8.29 $\pm$ 0.14	7.76 $\pm$ 0.22	-3.42		2MASS
Sgr09	12.090	10.570	9.420	7.00 $\pm$ 0.09	6.63 $\pm$ 0.15	-4.29		2MASS
Sgr10	12.045	10.367	9.048	6.37 $\pm$ 0.04	6.13 $\pm$ 0.10	-4.81		2MASS
Sgr11	11.219	10.058	9.448	8.29 $\pm$ 0.11	7.71 $\pm$ 0.13	-4.16		SAAO
Sgr12	13.258	11.599	10.182	6.78 $\pm$ 0.07	6.84 $\pm$ 0.20	-3.73		2MASS
Sgr13	11.424	10.298	9.724	8.78 $\pm$ 0.08		-3.91		SAAO
Sgr14	11.445	10.414	9.904	9.42 $\pm$ 0.11		-3.80		SAAO
Sgr15	13.363	11.331	9.701	6.01 $\pm$ 0.04	5.41 $\pm$ 0.06	-4.61	5.28	2MASS
Sgr16	14.644	12.555	10.685	5.70 $\pm$ 0.03	5.32 $\pm$ 0.07	-3.87	5.55	2MASS
Sgr17	11.874	10.511	9.526	7.87 $\pm$ 0.06		-4.08		SAAO
Sgr18	14.227	11.956	10.168	5.37 $\pm$ 0.03	4.80 $\pm$ 0.04	-4.46	4.63	2MASS
Sgr19	12.603	11.078	9.967	7.59 $\pm$ 0.08	7.05 $\pm$ 0.11	-3.73		SAAO
Sgr20	13.112	11.533	10.289	7.65 $\pm$ 0.07	6.35 $\pm$ 0.07	-3.48		2MASS
Sgr21	10.862	9.751	9.099	7.67 $\pm$ 0.07	7.87 $\pm$ 0.14	-4.52		SAAO
Sgr22	11.957	9.991	8.349	4.29 $\pm$ 0.01	3.36 $\pm$ 0.01	-5.92	3.03	2MASS
Sgr23	12.743	11.084	9.736	6.76 $\pm$ 0.07	5.75 $\pm$ 0.06	-4.13		2MASS
Sgr24	12.118	10.643	9.513	7.65 $\pm$ 0.11	6.98 $\pm$ 0.09	-4.17		2MASS
Sgr25	11.209	10.235	9.793	8.00 $\pm$ 0.04		-3.98		SAAO
Sgr26	11.303	10.359	9.882	8.82 $\pm$ 0.09		-3.89		SAAO
Sgr27	12.347	11.192	10.473	9.05 $\pm$ 0.13		-3.12		SAAO
Sgr28	11.424	10.401	9.961	8.42 $\pm$ 0.18		-3.78		SAAO
Sgr29	13.599	11.741	10.209	6.48 $\pm$ 0.07	6.38 $\pm$ 0.12	-3.90		2MASS
<b>Fornax</b>								
For1	14.722	13.262	12.120	9.53 $\pm$ 0.13		-5.18		2MASS
For2	16.106	14.525	12.879	9.56 $\pm$ 0.20		-4.76		2MASS
<b>Halo</b>								
Halo1	11.850	10.143	8.707	5.50 $\pm$ 0.03	4.74 $\pm$ 0.04	N/A	4.50	2MASS

cent Spitzer observations have yielded reliable determinations of mass-loss rates from AGB stars in these galaxies. We used the sample of carbon stars in the SMC presented by Lagadec et al. (2007), and in the LMC by Zijlstra et al. (2006). The mass-loss rates of these stars have been determined by Groenewegen et al. (2007) using a radiative transfer model. They give total mass-loss rates, using a gas-to-dust mass ratio of 200 and assuming an expansion velocity for all the stars in the sample of 10 km s<sup>-1</sup>.

We obtained the equivalent [9] and [11] magnitudes for the stars in the SMC and LMC sample by convolving the Spitzer IRS spectra with the response curves of the VISIR filters. The  $K$  magnitudes were taken from the Groenewegen et al. (2007) tabulation. The resulting relations for  $K_s - [9]$  and  $K_s - [11]$  versus mass-loss rate are shown in Fig. 5. The AGB stars in the Galaxy, SMC and LMC all follow the same trend on a  $K_s - [9]$  or  $K_s - [11]$  versus dust mass-loss rate relation. This appears not to depend on metal-

licity as what we measure is an optical depth and can be applied to derive the dust mass-loss rates for AGB stars in other galaxies.

The Spitzer spectra of LMC and SMC carbon stars show the presence of deep molecular absorption bands, together with the 11.3 $\mu\text{m}$  SiC emission band, making it difficult to define the continuum (Fig. 4). Zijlstra et al. (2006) define four narrow bands suitable for measuring the continuum for carbon stars. One of these (the 9.3 $\mu\text{m}$  band) is close to the transmission of the VISIR 9 $\mu\text{m}$  filter. This filter is in a region relatively free from strong molecular bands, apart from a possible C<sub>3</sub> band (Zijlstra et al. 2006), providing a metallicity-free mass-loss estimation. The second filter coincides with the 11.3 $\mu\text{m}$  band. The SiC band is known to be metallicity dependent, being weaker for lower metallicity stars (Lagadec et al. 2007). The  $K_s - [11]$  relation is therefore expected to have some metallicity dependence, but the SiC band does not dominate the spectrum in the same way as the silicate band does in oxygen-rich stars, and the dependence is therefore limited.

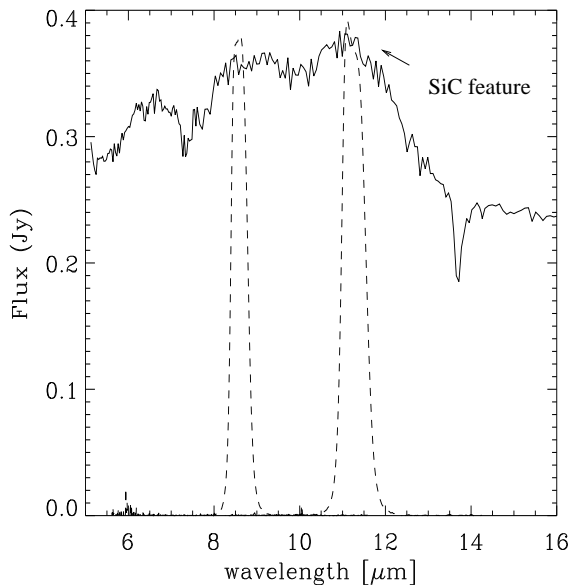


**Figure 4.** Spitzer spectrum of the C-rich SMC AGB star IRAS 00554 (Lagadec et al. 2007), superimposed with the VISIR PAH1 and PAH2 filters.

#### 4.1.2 Application

The  $K_s - [9]$  and  $K_s - [11]$  colours thus lead immediately to an estimation of the dust mass-loss rates in Sgr dSph and Fornax.

In this work, we assume that all the AGB stars observed are C-rich. This is likely given the low metallicities of Sgr dSph and Fornax, although we cannot rule out that a few stars in our sample might be O-rich. However, the relation between  $K_s - [9]$  or  $K_s - [11]$  and mass-loss rates are similar for C-rich and O-rich stars. We should keep in mind that the methods used to determine mass-loss rates in the Galaxy and the Magellanic Clouds are not direct measurements. The mass-loss rates in the Galaxy were calculated using the Jura (1987) formalism, which allows one to estimate the mass-loss rates for carbon stars using the observed IRAS  $60\mu\text{m}$  emission and measured expansion velocities. The mass-loss rates in the Magellanic Clouds have been determined using a radiative transfer model to fit mid-infrared spectra and near-infrared photometry, assuming a constant outflow velocity of  $10 \text{ km.s}^{-1}$ . These are the probably the most reliable estimates available. The  $[9]$  and  $[11]$  magnitudes are calculated from our VISIR observations and the derived dust mass-loss rates are listed in Table 3.

## 4.2 Method 2: radiative transfer models

To provide an alternative estimate for the mass-loss rates for these AGB stars, we also computed a grid of dust radiative transfer models using the DUSTY 1D code (Ivezić et al. 1999). For each model, the density distribution of a radiation-driven wind was assumed,  $\rho \sim r^{-1.8}$  (Elitzur & Ivezić 2001). For this choice, the DUSTY models compute the wind structure by solving the hydrodynamical equations as a set, coupled to the radiative transfer.

We assumed that the central star emits like a blackbody with  $T=2800\text{K}$ , a typical temperature for an AGB star. Previous papers have shown that in low metallicity galaxies, most of the mass-losing AGB stars are carbon-rich (e.g. van Loon et al. 1999a, Matsumura et al. (2002, 2005)). The dust in the stars we observed is

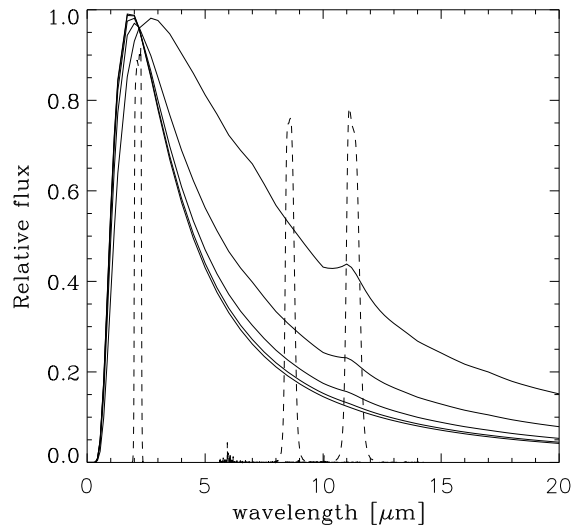


**Figure 6.** Spectral energy distribution of DUSTY models of carbon dust with different optical depths (respectively 0.01, 0.3, 1., 10. and 31. at  $1\mu\text{m}$ ), superimposed with the 2MASS  $K_s$  and VISIR PAH1 and PAH2 filters.

therefore likely to be carbonaceous and this is what we assume. Specifically, we assume that the dust grains are spherical and composed of a mixture of amorphous carbon (95%) and SiC (5%), with a grain size of  $0.1\mu\text{m}$ . The optical properties of these grains are calculated using Hanner (1988) and Pégourié (1988) respectively. We assumed that the dust temperature at the inner boundary is  $1000\text{K}$ . The shell thickness (i.e. the ratio between the outer and inner radius) is set to  $10^4$ .

The optical depth of the envelope is proportional to the dust mass-loss rate. We can thus associate a mass-loss rate with a model of a given optical depth. The output of these DUSTY models contains values of the total mass-loss rate (dust+gas) and of the shell expansion velocity. As stated above, we prefer to discuss dust mass-loss rates. We convert the total mass-loss rates to dust-mass loss rates by dividing by the gas-to-dust mass ratio. We, however, have to keep in mind that the expansion velocity also depends on the dust-to-gas ratio, rendering the total mass-loss rate less than straightforward to measure.

We thus calculated a benchmark of DUSTY models with these input parameters and different optical depths. The outputs of these models are spectra which we convolved with the 2MASS  $K_s$  and VISIR PAH1 and PAH2 filters (Fig. 6) to determine the  $K_s - [9]$  and  $K_s - [12]$  colours associated with the different models.

Using these models, we find these relations between colours and dust mass-loss rates:

$$\log(\dot{M}_{\text{dust}}) = -8.14 \times ((K_s - [9]) - 0.97)^{-0.06} \times 0.75 \log(L/10^4) \quad (6)$$

$$\log(\dot{M}_{\text{dust}}) = -8.28 \times ((K_s - [11]) - 0.98)^{-0.07} \times 0.75 \log(L/10^4) \quad (7)$$

where  $L$  is the luminosity of the star in units of solar luminosity. The measured colours then directly give us an estimation of the mass-loss rates using relation (6) and (7). The resulting values are listed Table 3.

## 4.3 Comparison

Both methods should only be used for the colour range for which they are defined. This is especially true for blue stars, where the

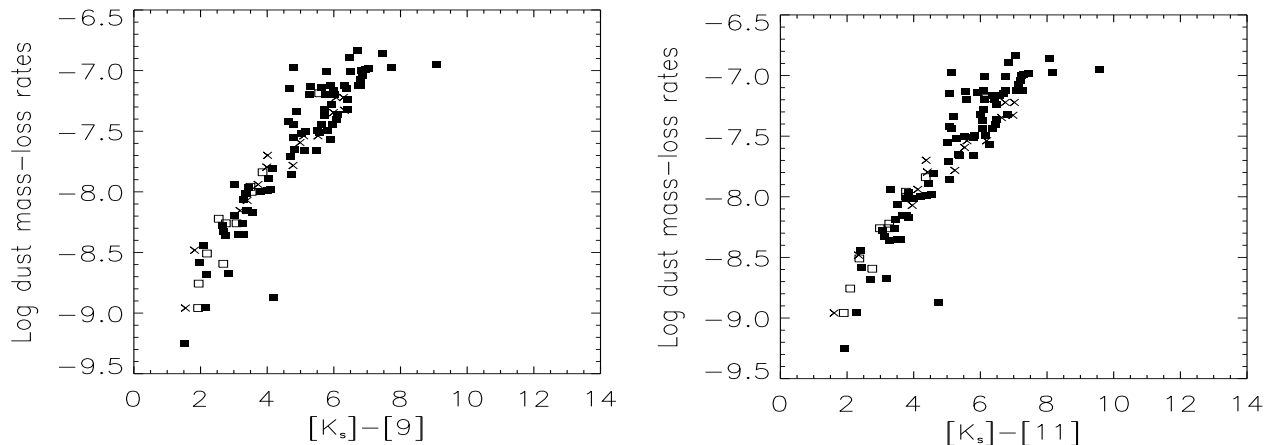


**Figure 5.** Dust mass-loss rates of C-rich AGB stars as a function of  $K - [9]$  (left) and  $K - [11]$  (right) colours of stars from the sample in Whitelock et al. (2006) (Galaxy, black squares), Lagadec et al. (2007) (SMC, open squares) and Zijlstra et al. (2006) (LMC, crosses).

mass-loss rates do not go to zero for photospheric colours (as it is a logarithmic equation). We choose to set mass-loss rates for stars with  $K_s - [9] < 0.8$  to zero. This affects the three bluest stars: Sgr06, Sgr13 and Sgr14.

Variability introduces an uncertainty. For the stars with WMIF names, the  $K$ -band magnitudes are averaged over the variability. For the others, they are single-epoch values which may differ from the mean: the amplitude at  $K$  is typically 0.1 mag for blue stars and can be up to 1 mag or possibly more for red stars. Finally, the VISIR photometry may also be affected by stellar variability. Indeed little is known about the variability in the mid-infrared of carbon AGB stars. Observations of a sample of 23 C-rich AGB stars (Le Bertre 1992) have shown that the amplitude of variation of the observed stars from 1 to  $20\mu\text{m}$  seems to decrease with wavelength. Both effects (near-infrared and mid-infrared variability) will affect all four methods in the same way.

The different methods also show internal differences. Fig. 7 shows the comparison. The left panels compare mass-loss rates derived from the colours (method 1) with those from the models (method 2). A systematic offset can be seen, with the DUSTY models giving a higher mass-loss rate by up to a factor of 1.5. The right panels compare the mass-loss rates derived from the two different filters used, where the agreement is good. There is a small offset seen in the model results, where the mass-loss rates derived using  $[11]$  are a little higher than those derived from  $[9]$ . The offset amounts to about 10 per cent. This may be due to a contribution from SiC at  $11\mu\text{m}$ .

The first aim of our DUSTY model was to check the validity of our mass-loss rates determination method based on infrared colours. The fact that both methods give very similar results thus indicates that this method is a good estimator of AGB stars dust-mass loss rates.

## 5 DISCUSSION

### 5.1 Mass-loss rates

The first main result of this study is that most of the observed stars in Sgr dSph (29 stars) and Fornax (2 stars) are red in  $K_s - [9]$ , indicating the presence of a dusty envelope and dusty mass loss. The

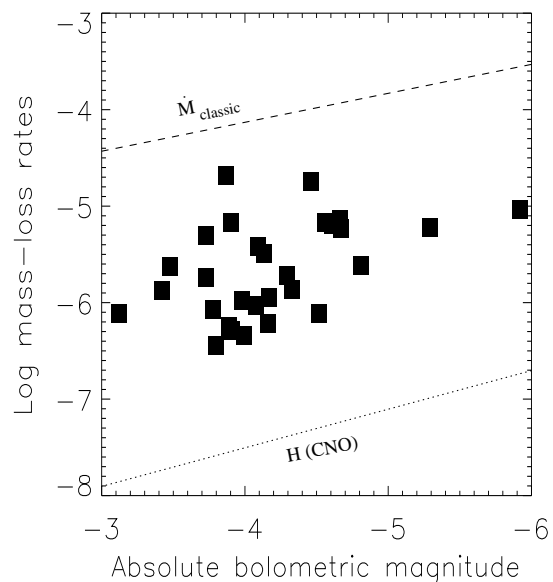


**Figure 8.** Total (gas+dust) mass-loss rate as a function of the absolute bolometric magnitude.

dust mass-loss rates are in the range  $5 \times 10^{-10}$  to  $3 \times 10^{-8} M_{\odot} \text{yr}^{-1}$  for the AGB stars in Sgr dSph and around  $5 \times 10^{-9} M_{\odot} \text{yr}^{-1}$  for those in Fornax. A number of Sgr dSph stars have  $K_s - [9] < 1$ , and these are probably photospheric colours.

Our observations indicate that even at very low metallicities ( $[\text{Fe}/\text{H}] \sim -0.9$ , see Section 2.2), as found in the Fornax dwarf spheroidal galaxy, dusty mass-loss occurs.

The mass-loss rates we have derived are *dust* mass-loss rates. To give constraints to stellar evolution codes, one needs to know the total (gas+dust) mass-loss rate. For that we need to know the dust-to-gas mass ratio  $\psi$ , which is not well known even for Galactic AGB stars. For example, for IRC+10216, the best studied AGB star, values in the range 170-700 are found in the literature (Mensh'chikov et al. 2001). It is obviously difficult to determine



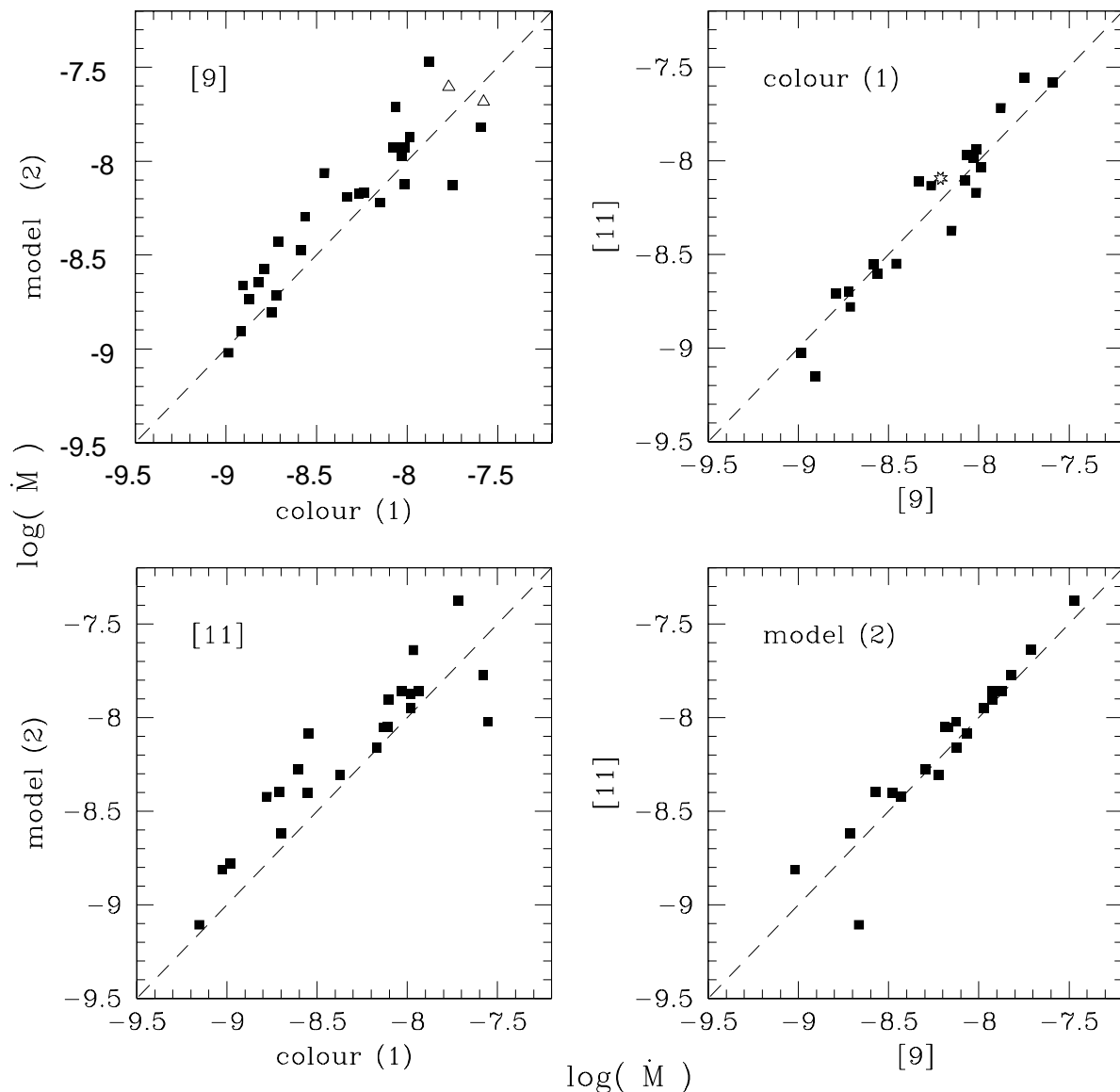


**Figure 7.** Comparison between the different determinations of the dust mass-loss rate. The left panels plot the rates determined from the colour method (method 1) against those from the DUSTY models (method 2), for the two VISIR filters. The right panels compare the rates derived from the two different filters, for each of the methods. Squares are Sgr dSph stars, triangles Fornax and the star symbol is the Galactic halo star.

this ratio in other galaxies. van Loon (2006) argue that the ratio scales linearly with the metallicity. This can be simply understood by the fact that at low metallicity, fewer seeds for dust formation are available and thus dust formation is less efficient. They therefore assume that:

$$\psi = \psi_{\odot} 10^{-[\text{Fe}/\text{H}]} \quad (8)$$

, where  $\psi_{\odot} = 0.005$  (van Loon et al. 2005).

If we assume  $[\text{Fe}/\text{H}] = -0.55$  for Sgr dSph (Dudziak et al. 2000), then for the AGB stars in this galaxy,  $\psi \sim 1.4 \times 10^{-3}$ . Assuming  $[\text{Fe}/\text{H}] = -0.9$  for Fornax leads to an estimate of the dust-to-gas mass ratio  $\psi \sim 6.3 \times 10^{-4}$ . This will provide total mass-loss rates of 700 and 1600 times, respectively, higher than the dust mass-loss rates in Sgr dSph and Fornax. Note, however, that these are upper limits, as the dust expansion velocity is probably smaller in these galaxies, as well as the drift velocity, but no obser-

vations have yet been made that measure the expansion velocities of carbon star at low metallicities.

The assumption of a linear relation between dust production and metallicity can be questioned. For carbon stars, the two main dust components are amorphous carbon dust (soot) and silicon carbide. The abundance of the latter is limited by Si which is not produced in AGB stars. However, amorphous carbon depends only on the carbon abundance, which is strongly enriched via third dredge-up. The amount of carbon dust may still depend on the number of available seeds (e.g. TiC) which can introduce a metallicity dependence, but it is less likely to be a linear one.

**Table 3.** Mass-loss rates determined from our VISIR observations.  $\dot{M}_1$  and  $\dot{M}_2$  are the dust mass-loss rates (in  $M_{\odot}\text{yr}^{-1}$ ) derived from method 1, using the [9] and [11] colours respectively.  $\dot{M}_3$  and  $\dot{M}_4$  are the dust mass-loss rates (in  $M_{\odot}\text{yr}^{-1}$ ) derived from method 2, using the [9] and [11] colours respectively.

Star number	$K_s$ -[9]	$K_s$ -[11]	$\dot{M}_1$	$\dot{M}_2$	$\dot{M}_3$	$\dot{M}_4$
<b>Sgr dSph</b>						
Sgr01	3.74	4.11	$1.0 \times 10^{-8}$	$9.2 \times 10^{-9}$	$1.4 \times 10^{-8}$	$1.5 \times 10^{-8}$
Sgr02	3.56	4.28	$8.6 \times 10^{-9}$	$1.1 \times 10^{-8}$	$2.1 \times 10^{-8}$	$2.4 \times 10^{-8}$
Sgr03	3.53	3.94	$8.4 \times 10^{-9}$	$7.9 \times 10^{-9}$	$1.3 \times 10^{-8}$	$1.4 \times 10^{-8}$
Sgr04	2.00	2.30	$1.9 \times 10^{-9}$	$1.7 \times 10^{-9}$	$3.9 \times 10^{-9}$	$3.9 \times 10^{-9}$
Sgr05	3.08	3.40	$5.4 \times 10^{-9}$	$4.7 \times 10^{-9}$	$7.2 \times 10^{-9}$	$7.2 \times 10^{-9}$
Sgr06	0.75	1.80	$6.6 \times 10^{-10}$	$1.0 \times 10^{-9}$	blue	$1.6 \times 10^{-9}$
Sgr07	3.68	4.36	$9.7 \times 10^{-9}$	$1.2 \times 10^{-8}$	$1.3 \times 10^{-8}$	$1.5 \times 10^{-8}$
Sgr08	1.98	2.51	$1.9 \times 10^{-9}$	$2.0 \times 10^{-9}$	$2.0 \times 10^{-9}$	$2.5 \times 10^{-9}$
Sgr09	2.37	2.74	$2.7 \times 10^{-9}$	$2.5 \times 10^{-9}$	$5.3 \times 10^{-9}$	$5.5 \times 10^{-9}$
Sgr10	2.62	2.86	$3.5 \times 10^{-9}$	$2.8 \times 10^{-9}$	$9.1 \times 10^{-9}$	$8.7 \times 10^{-9}$
Sgr11	1.10	1.68	$8.7 \times 10^{-10}$	$9.4 \times 10^{-10}$	$3.0 \times 10^{-10}$	$1.5 \times 10^{-9}$
Sgr12	3.35	3.29	$7.0 \times 10^{-9}$	$4.2 \times 10^{-9}$	$6.4 \times 10^{-9}$	$5.3 \times 10^{-9}$
Sgr13	0.89		$7.3 \times 10^{-10}$		blue	
Sgr14	0.43		$5.2 \times 10^{-10}$		blue	
Sgr15	3.64	4.24	$9.3 \times 10^{-9}$	$1.0 \times 10^{-8}$	$1.3 \times 10^{-8}$	$1.5 \times 10^{-8}$
Sgr16	4.93	5.31	$3.0 \times 10^{-8}$	$2.6 \times 10^{-8}$	$1.2 \times 10^{-8}$	$1.3 \times 10^{-8}$
Sgr17	1.60		$1.3 \times 10^{-9}$		$1.9 \times 10^{-9}$	
Sgr18	4.74	5.31	$2.6 \times 10^{-8}$	$2.6 \times 10^{-8}$	$1.7 \times 10^{-8}$	$1.9 \times 10^{-8}$
Sgr19	2.32	2.86	$2.6 \times 10^{-9}$	$2.8 \times 10^{-9}$	$3.5 \times 10^{-9}$	$4.1 \times 10^{-9}$
Sgr20	2.58	3.88	$3.4 \times 10^{-9}$	$7.5 \times 10^{-9}$	$3.5 \times 10^{-9}$	$6.0 \times 10^{-9}$
Sgr21	1.37	1.17	$1.1 \times 10^{-9}$	$6.1 \times 10^{-10}$	$1.5 \times 10^{-9}$	$3.0 \times 10^{-10}$
Sgr22	4.00	4.93	$1.3 \times 10^{-8}$	$1.9 \times 10^{-8}$	$3.8 \times 10^{-8}$	$4.7 \times 10^{-8}$
Sgr23	2.92	3.93	$4.7 \times 10^{-9}$	$7.8 \times 10^{-9}$	$6.8 \times 10^{-9}$	$9.5 \times 10^{-9}$
Sgr24	1.81	2.48	$1.6 \times 10^{-9}$	$1.9 \times 10^{-9}$	$2.8 \times 10^{-9}$	$4.1 \times 10^{-9}$
Sgr25	1.74		$1.5 \times 10^{-9}$		$2.2 \times 10^{-9}$	
Sgr26	1.01		$8.1 \times 10^{-10}$	$4.6 \times 10^{-11}$		
Sgr27	1.36		$1.1 \times 10^{-9}$		$5.6 \times 10^{-10}$	
Sgr28	1.48		$1.2 \times 10^{-9}$		$1.2 \times 10^{-9}$	
Sgr29	3.67	3.77	$9.6 \times 10^{-9}$	$6.7 \times 10^{-9}$	$8.3 \times 10^{-9}$	$7.6 \times 10^{-9}$
<b>Fornax</b>						
For1	2.59		$3.4 \times 10^{-9}$		$1.1 \times 10^{-8}$	
For2	3.32		$6.9 \times 10^{-9}$		$1.2 \times 10^{-8}$	
<b>Halo</b>						
Halo1	3.21	3.97	$6.1 \times 10^{-9}$	$8.1 \times 10^{-9}$	N/A	N/A

## 5.2 Evolution

For a better understanding of the evolution of these AGB stars, it is interesting to compare the measured mass-loss rates with the rate at which mass is consumed by nuclear burning  $\dot{M}_{\text{nuc}}$ . Most of the energy in AGB stars comes from CNO burning in the H burning shell. This reaction releases  $\sim 6.1 \times 10^{18} \text{ erg g}^{-1}$ .  $\dot{M}_{\text{nuc}}$  is proportional to the luminosity,  $L$ . Fig. 8 shows the measured mass-loss rates as a function of the luminosity. Over-plotted are the  $\dot{M}_{\text{nuc}}$  vs  $L$  relation and the classical single-scattering limit  $\dot{M}_{\text{classic}} = L(v_{\text{exp}})^{-1} \propto L^{0.75}$  vs  $L$ . This diagram clearly indicates that all the measured mass-loss rates are below the classical single-scattering limit. Thus no multiple scattering of photons by dust in the envelope is needed to explain the observed mass-loss rates as can be necessary for the very high mass-loss rates measured for some Galactic AGB stars. Note though, that extremely high mass-loss rates are rare even in the Galaxy where they are thought to represent the brief end of the most massive AGB stars. It is hardly surprising that nothing similar has been found within our

incomplete sample of stars in small galaxies which are not generally believed to have an intermediate mass population.

The measured mass-loss rates are all above the  $\dot{M}_{\text{nuc}}$  line. This has important consequences for the evolution of these stars. Their evolution will terminate when the mantle becomes depleted by mass-loss long before the nuclear burning core can grow significantly. Similar conclusions were reached about AGB stars in the LMC (van Loon et al. 1999b). This is independent on the value of  $\psi$  we assume as the measured mass-loss rates are more than one order of magnitude higher than the nuclear burning rates.

The mass-loss rate versus bolometric luminosity diagram shows that most of the stars fall within the range  $4 \times 10^{-7} < \dot{M} < 6 \times 10^{-6}$  and  $-3.4 < M_{\text{bol}} < -4.5$ . Jackson et al. (2007) observed stars with the same bolometric magnitudes and mass-loss rates in the low metallicity Local Group galaxy WLM ([Fe/H]  $\sim -1.13$ ). Stars with similar luminosities and mass-loss rates have also been observed in the Large Magellanic Cloud (van Loon et al. 1999b). These authors have pointed out, from dynamical

considerations following Gail & Sedlmayr (1987), that dust-driven winds below a few  $10^{-6} M_{\odot} \text{yr}^{-1}$  with luminosities around a few  $10^3 L_{\odot}$  should not exist. Our observations thus disagree with those predictions.

### 5.3 Comparison with mass-losing AGB stars in other galaxies

To compare the mass-loss rates we measured in Fornax and Sgr dSph with mass-loss rates from AGB stars in the Magellanic Clouds (MCs) (thus in more metal-rich galaxies), we used the mass-loss rates derived by Groenewegen et al. (2007) for AGB stars in the MCs. To obtain an unbiased estimation of the bolometric magnitudes in these four galaxies, we determined it for the MCs sample in the same way we did for Fornax en Sgr dSph (using the JHK magnitudes and relation 1). The resulting relation between mass-loss rates and bolometric magnitude for these four galaxies is shown in Fig.9.

The first conclusion is that Fornax AGB stars, thus stars with very low metallicities, have quite small dust mass-loss rates for their luminosities. The smallest mass-loss rates are observed for less luminous, more metal-rich AGB stars in Sgr dSph and the SMC, but it is likely that Fornax has lower mass-loss rate AGB stars too weak to be detected.

For stars in the LMC the mass-loss rates are already high for a bolometric magnitude around  $-4$  and then constant or even slightly decreasing. Note that two stars are outliers with  $M_{\text{bol}}$  around  $-5.5$  and  $\log(\text{dust mass-loss rates})$  around  $-9$  and  $-8.5$ . For stars in the SMC, the dust mass-loss rates increase steadily from  $M_{\text{bol}} \sim -4.5$  to  $\sim -5$ . For  $M_{\text{bol}} \sim -5$ , the observed mass-loss rates are of the same order of magnitude in the LMC and SMC. Stars in Sgr dSph show a similar behaviour, but the mass-loss rates begin to increase at  $M_{\text{bol}} \sim -4$ . The fact that the mass-loss rates are high for lower luminosity in the LMC than in the other galaxies could be explained by the higher metallicity of the LMC with respect to the three other galaxies. It has been shown that at lower metallicity, stars become carbon-rich earlier on the AGB (e.g., Lagadec et al. 2007). So AGB stars become C-rich later in the LMC. The superwind might thus begin when the stars become carbon rich in the LMC, while the stars might be C-rich well before the onset of the superwind in the lower metallicity galaxies. The two Sgr dSph stars with the highest mass-loss rates and  $M_{\text{bol}} \sim -4$  (Sgr16 and Sgr18) would thus be stars where the superwind phase necessary to explain the densities seen in typical planetary nebulae (Renzini 1981) has already begun.

If we compare the dust mass-loss rates for a given luminosity, then metallicity effects seem to appear. Indeed, for a given bolometric magnitude fainter than  $-4.5$ , stars in the Sgr dSph and the SMC seem to have a smaller mass-loss rate than stars in the LMC. This could be due to the fact that Sgr dSph and the SMC have a smaller metallicity than the LMC and that at low luminosity less dust is formed in these galaxies than in the LMC, leading to a lower radiation pressure on dust grains and thus smaller mass-loss rates. Observations of a bigger sample of AGB stars in different galaxies are however needed to confirm this. Indeed our MCs sample has been selected from the MSX catalogue (Egan et al. 2001) and is thus limited to stars brighter than 45 mJy in the MSX A band ( $8.3 \mu\text{m}$ ), preventing us to study the very early AGB. In Fornax we observed the brightest MIR stars while Sgr dSph stars were selected from NIR colors and sample the full AGB. Observations of fainter MCs stars in the MIR would enable us to study stars with fainter bolometric magnitude (with  $-4 < M_{\text{bol}} < -3$ ) and compare it with some early AGB Sgr dSph stars we observed.

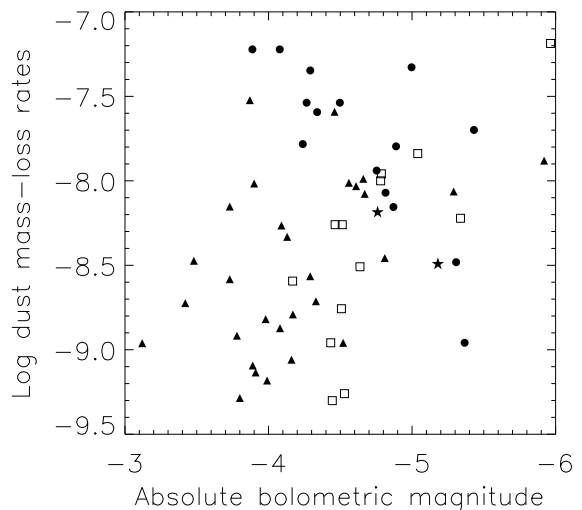


**Figure 9.** Dust mass-loss rates as a function of bolometric magnitude for stars in Sgr dSph (triangles), Fornax (stars), LMC (circles) and SMC (Squares).

## 6 CONCLUSIONS

We have presented a study of mass-loss from AGB stars in the Sagittarius and Fornax dwarf spheroidal galaxies using mid-infrared photometry obtained with VISIR (VLT, ESO).

We have shown that the well known relation between  $K - [12]$  colours and mass-loss rates among Galactic stars is also valid for AGB stars in lower metallicity galaxies. We used this relation and radiative transfer models to estimate dust mass-loss rates for 15 stars in Sgr dSph and 2 stars in Fornax.

Our study showed that some AGB stars in the Sgr dSph and Fornax galaxies are losing mass. The estimated dust mass-loss rates are in the range  $5 \times 10^{-10}$  to  $3 \times 10^{-8} M_{\odot} \text{yr}^{-1}$  for the stars in Sgr dSph and around  $5 \times 10^{-9} M_{\odot} \text{yr}^{-1}$  for those in Fornax. The values obtained with the two different methods are of the same order of magnitude. These mass-loss rates are higher than the nuclear burning rates, so these stars will terminate their AGB evolution by the depletion of their stellar mantles, before their cores can grow significantly.

Using previous work to get an estimation of the dust-to-gas mass ratio for the stars observed we found that most of them had very low mass-loss rates for their luminosity. This is in contradiction with theoretical predictions (see e.g Gail & Sedlmayr 1987).

## ACKNOWLEDGMENTS

E.L. acknowledges support from a PPARC rolling grant. We thank the referee, Joris Blommaert, for his useful comments that helped improving the quality of the paper.

## REFERENCES

- Bellazzini, M., Ferraro, F. R., Pancino, E. 2001. ApJ, 556, 635
- Bellazzini, M., Correnti, M., Ferraro, F. R., Monaco, L., & Montegriffo, P. 2006, A&A, 446, L1
- Bersier, D. 2000, ApJ, 543, L23

- Bonifacio, P., Sbordone, L., Marconi, G., Pasquini, L., Hill, V. 2004. *A&A*, 414, 503
- Bowen, G. H., & Willson, L. A. 1991, *ApJ*, 375, L53
- Carpenter, J. M. 2001, *AJ*, 121, 2851
- Cutri, R. M., et al. 2003, The IRSA 2MASS All-Sky Point Source Catalog, IPAC/CIT (2MASS)
- de Laverny, P., Abia, C., Domínguez, I., Plez, B., Straniero, O., Wahlin, R., Eriksson, K., Jørgensen, U. G. 2006. *A&A*, 446, 1107
- Dudziak, G., Péquignot, D., Zijlstra, A. A., & Walsh, J. R. 2000, *A&A*, 363, 717
- Egan, M. P., Van Dyk, S. D., & Price, S. D. 2001, *AJ*, 122, 1844
- Gail, H.-P., & Sedlmayr, E. 1987, *A&A*, 177, 186
- Groenewegen, M. A. T., et al. 2007, *MNRAS*, 376, 313
- Hanner, M. 1988, *Infrared Observations of Comets Halley and Wilson and Properties of the Grains*, 22
- Höfner, S., Jørgensen, U. G., Loidl, R., & Aringer, B. 1998, *A&A*, 340, 497
- Ivezic, Z., Nenkova, M., & Elitzur, M., User manual for DUSTY, University of Kentucky internal report
- Jackson, D. C., Skillman, E. D., Gehrz, R. D., Polomski, E., & Woodward, C. E. 2007, *ApJ*, 656, 818
- Jura, M. 1987, *ApJ*, 313, 743
- Lagadec, E., et al. 2007, *MNRAS*, 376, 1270
- Lagage, P. O., et al. 2004, *The Messenger*, 117, 12
- Law, D. R., Johnston, K. V., Majewski, S. R. 2005. *ApJ*, 619, 807
- Layden, A. C., & Sarajedini, A. 2000, *AJ*, 119, 1760
- Le Bertre, T. 1992, *A&AS*, 94, 377
- Loup, C., Forveille, T., Omont, A., & Paul, J. F. 1993, *A&AS*, 99, 291
- Le Bertre, T. 1997, *A&A*, 324, 1059
- Maeder, A. 1992, *A&A*, 264, 105
- Majewski, S. R., Skrutskie, M. F., Weinberg, M. D., & Ostheimer, J. C. 2003, *ApJ*, 599, 1082
- Mateo, M., Kubiak, M., Szymanski, M., Kaluzny, J., Krzeminski, W., & Udalski, A. 1995, *AJ*, 110, 1141
- Matsuura, M., et al. 2007, *MNRAS*, in press, astro-ph 0709.3199
- Matsuura, M., et al. 2005, *A&A*, 434, 691
- Matsuura, M., Zijlstra, A. A., van Loon, J. T., Yamamura, I., Markwick, A. J., Woods, P. M., & Waters, L. B. F. M. 2002, *ApJL*, 580, L133
- Mauron, N., Azzopardi, M., Gigoyan, K., & Kendall, T. R. 2004, *A&A*, 418, 77
- Men'shchikov, A. B., Balega, Y., Blöcker, T., Osterbart, R., & Weigelt, G. 2001, *A&A*, 368, 497
- Pégourié, B. 1988, *A&A*, 194, 335
- Pont, F., Zinn, R., Gallart, C., Hardy, E., Winnick, R. 2004, *AJ*, 127, 840
- Renzini, A. 1981, *Astrophysics and Space Science Library*, 89, 319
- Rieke, G. H., & Lebofsky, M. J. 1985, *ApJ*, 288, 618
- Saviane, I., Held, E. V., Bertelli, G. 2000. *A&A*, 355, 56
- van Loon, J. T., Zijlstra, A. A., & Groenewegen, M. A. T. 1999a, *A&A*, 346, 805
- van Loon, J. T., Groenewegen, M. A. T., de Koter, A., Trams, N. R., Waters, L. B. F. M., Zijlstra, A. A., Whitelock, P. A., & Loup, C. 1999b, *A&A*, 351, 559
- van Loon, J. T. 2000, *A&A*, 354, 125
- van Loon, J. T., Marshall, J. R., & Zijlstra, A. A. 2005, *A&A*, 442, 597
- van Loon, J. T. 2006, arXiv:astro-ph/0612374
- Venn, K. A. 1999, *ApJ*, 518, 405
- Whitelock, P. A., Irwin, M., Catchpole, R. M. 1996, *New Ast.*, 1, 57
- Whitelock, P., Menzies, J., Feast, M., Marang, F., Carter, B., Roberts, G., Catchpole, R., & Chapman, J. 1994, *MNRAS*, 267, 711
- Whitelock, P., Menzies, J., Irwin, M., & Feast, M. 1999, *IAU Symposium*, 192, 136
- Whitelock, P. A., Feast, M. W., Marang, F., & Groenewegen, M. A. T. 2006, *MNRAS*, 369, 751
- Zijlstra, A. A. 2004, *MNRAS*, 348, L23
- Zijlstra, A. A., et al. 2006b, *MNRAS*, 370, 1961
- Zijlstra, A. A., Gesicki, K., Walsh, J. R., Péquignot, D., van Hoof, P. A. M., Minniti, D. 2006a, *MNRAS*, 369, 875